Facets, indium distribution, and lattice distortion of InGaAs/GaAs quantum dots observed by three-dimensional scanning transmission electron microscope

Kazunari Ozasa,[a] Yoshinobu Aoyagi, and Masaya Iwaki
The Institute of Physical and Chemical Research (RIKEN), 2-1 Hirosawa, Wako, Saitama 351-0198, Japan

Hiroki Kurata
Institute for Chemical Research, Kyoto University, Gokasho, Uji, Kyoto 611-0011, Japan

(Received 16 December 2002; accepted 14 March 2003)

Multiazimuth 360° observation of InGaAs/GaAs quantum dots (QDs) was performed with a 300 kV scanning transmission electron microscope, where both cross-sectional and plan-view images of the same specific QDs can be taken for a single specimen. The facet structure of truncated pyramids was reconstructed from facet-enhanced bright-field images newly observed with the incident axes slightly off from $\langle -552 \rangle$ or $\langle -332 \rangle$, resulting in high contrast for the lattice distortion on (110) facets of InGaAs QDs. Dark-field images for a large QD clearly indicate indium distribution inside the large QD, originating from the coalescence of two small QDs during growth. Localized relaxation of the lattices was observed, for the same large QD with indium content fluctuation, as disturbed/disappeared moire-fringes in the images taken with the incidence around $\langle -552 \rangle$.
 [DOI: 10.1063/1.1572976]

I. INTRODUCTION

Investigation of the optical and electrical properties of quantum dots (QDs) has revealed detailed carrier dynamics in QDs,[1–5] in which atomic-scale information on QD shapes, chemical composition, and lattice distortion[6–12] are required in three dimensions for further theoretical calculations of quantum effects in QDs. In order to obtain such atomic-scale information for epitaxially grown semiconductor QDs, one of the most effective ways is to employ a transmission electron microscope (TEM). Facet images of large QDs[11,13–15] and misfit dislocations[16–20] have been reported based on TEM observations. The largest disadvantage of conventional TEM observations, however, is that one cannot obtain three-dimensional (3D) images of specific QDs but only either plan-view images or cross-sectional images, depending on the specimen structure prepared. The facets of QDs and dislocations have been discussed mainly based on cross-sectional images,[17,19,20] whereas distribution of QDs and moire fringes can be observed easily in plan-view images.[16,18] Obviously, such exclusive observation results in limitations on the comprehensive understanding of the QD shapes, chemical compositions, and lattice distortions.

The disadvantage of conventional TEM observations can be overcome if one can prepare a fine cylindrical specimen and observe it three dimensionally with specimen rotation.[21,22] In this paper, we describe the realization of 3D scanning transmission electron microscope (STEM) observation of such a cylindrical specimen of InGaAs/GaAs QDs. The facet-enhanced images were obtained with the unconventional incident axes found in this study, and the facet structure of QDs was reconstructed from the images. The direct observation of indium content fluctuation and correlated lattice distortion on the same specific large QD was presented.

II. EXPERIMENT

The QDs of $In_{0.5}Ga_{0.5}As$ were prepared on a GaAs(001) substrate with the conventional strain-induced self-assembly technology. Chemical beam epitaxy was employed to grow InGaAs at 480 °C, using triethylgallium (TEGa), trimethylindium (TMIn), and precracked AsH_3.[23,24] The diameter, height, and density of the QDs measured using an atomic force microscope were 34 ± 6 nm, 3-5 nm, and $6.9 \times 10^{10}\,cm^{-2}$, respectively. The QDs were capped by amorphous Si (*a*-Si) by electron-beam deposition at room temperature. The selection of *a*-Si rather than GaAs for capping is to emphasize the interface of the QDs/capping layer in STEM images by the difference in crystallinity, i.e., single crystal versus amorphous.

One of the key issues to realize 3D-STEM observation is the preparation of a fine cylindrical specimen, which contains the interface of QDs/capping layer along its rotation axis. We achieved it using a type of micromachine technique; i.e., focused ion beam (FIB) and microsampling[21,25] for cutting, mounting, and thinning the specimen. A small piece (cube with side length approximately $10-15\,\mu m^2$) of the sample including the QDs/capping interface was quarried out from the sample surface and mounted on a metal (Mo) cylinder base (0.9 mm diameter, 3.9 mm long). In order to perform both the plan-view and cross-sectional observations, the $\langle 331 \rangle$ direction of the piece was adjusted to the rotation axis of the cylinder base, as shown in Fig. 1(a). The choice of $\langle 331 \rangle$ instead of the $\langle 110 \rangle$ direction for the specimen rotation axis is to observe the QDs slightly off the $\langle 11n \rangle$ family axes such as $\langle 0-13 \rangle$. By annular sputtering from the $\langle 110 \rangle$ direction with 30 kV Ga^+ FIB (Hitachi FB-2000A), the piece was thinned down below 300 nm diameter. Figure

[a]Electronic mail: ozasa@postman.riken.go.jp

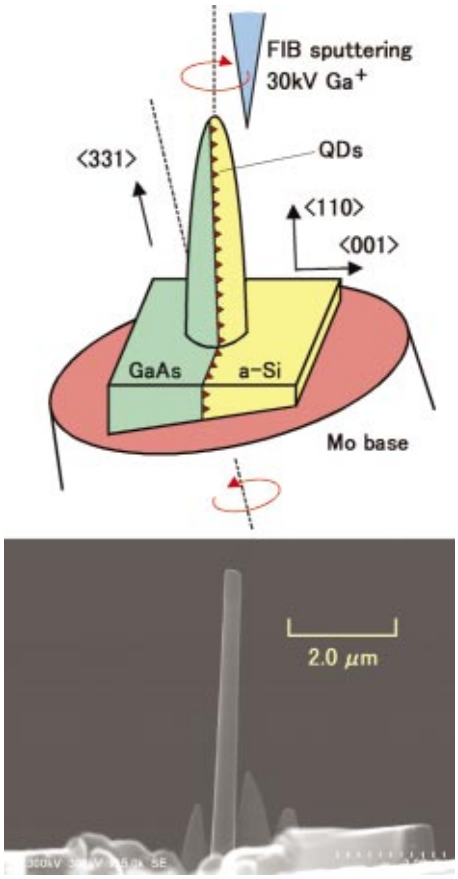

FIG. 1. (Color) Schematic of cylindrical specimen with designed axis alignment (top) and scanning electron micrograph of the prepared specimen (bottom).

1(b) shows the fabricated cylindrical specimen, which was approximately 200-300 nm thick. The length of the cylinder was approximately 5 μm, sufficiently large to search low-density defects. A detailed description of the specimen fabrication will be reported separately.[26]

The specimen was mounted on a holder with a pulse-motor-driven specimen-rotation mechanism for 360° observation with a fixed rotation axis ($\langle 331 \rangle$ direction in this case), or on a two-axis tilting holder with better incidence alignment but a limited rotation range of $\pm 20°$. The two holders were designed to fit the conventional TEM/STEM system (Hitachi HF-3000). For 3D observation, STEM was preferred to TEM because of its lower chromatic aberration for specimens thicker than 100 nm. The STEM system was operated with a 300 kV field-emission electron beam (typically 10–30 μA), and equipped with two alternative electron detectors; one for bright field images (<1.0 mrad) and the other, which is a high-angle annular detector with a detection angle of 40–200 mrad, for dark-field images. The ultimate STEM space resolution was estimated to be less than 0.5 nm.

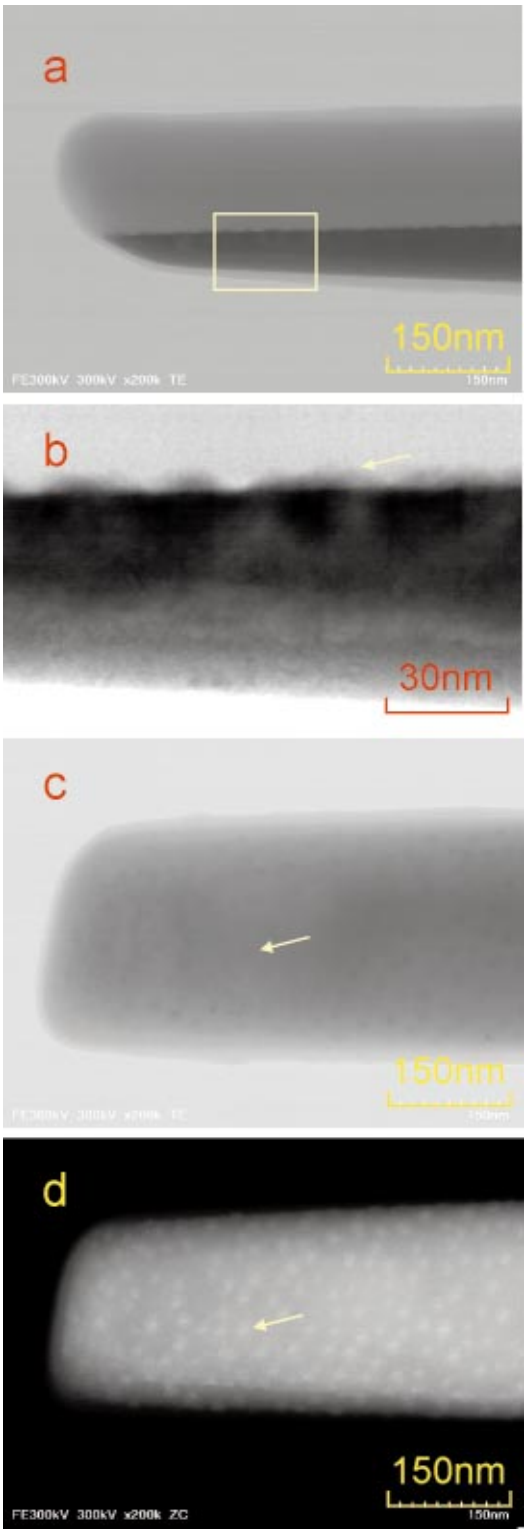

FIG. 2. (Color) STEM images taken with (a) and (b) $\langle -110 \rangle$ incidence (bright field), (c) approximately $\langle -1-16 \rangle$ (bright field), and (d) approximately $\langle -1-16 \rangle$ (HAADF image) incidence. Arrows indicate that the same specific QD can be traced with specimen rotation.

III. RESULTS AND DISCUSSION

A. Cross-sectional and plan-view STEM observations

The cross-sectional STEM bright field image of the cylindrical specimen is shown in Fig. 2(a), taken with $\langle -110 \rangle$ incidence. The QDs were observed at the interface of InGaAs/GaAs and *a*-Si, as hemispheres gently sloping at their edges, 6–7 nm in height and approximately 22 nm in base diameter [Fig. 2(b)]. In spite of the difference in specimen structure/preparation, the images of the QDs obtained with the cylindrical specimen are similar in quality to those

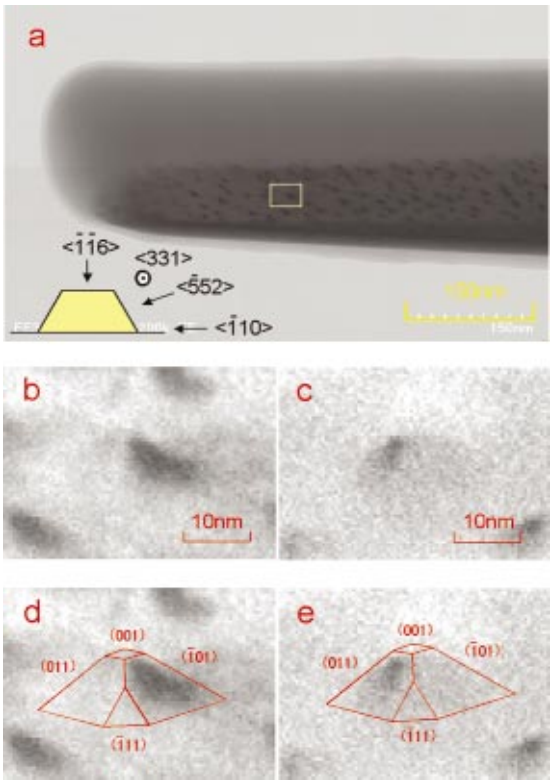

FIG. 3. (Color) Facet-enhanced STEM image (a)–(c) and reconstructed facet pyramid (d) and (e). (a), (b), and (d) 20°-rotated, and (c) and (e) 26°-rotated from $\langle -110\rangle$. The inset in (a) illustrates the observation direction in $\langle 331\rangle$ projection image of QD.

obtained with the conventional thin-film specimen. A thin damage layer (approximately 10 nm) formed by the FIB process was observed at the surface of specimen, but it has little effects on the STEM observation.

By rotating the cylindrical specimen 90° from the cross-sectional incidence, plan-view images can be observed as shown in Fig. 2(c). Since the rotation axis was designed to be $\langle 331\rangle$, the incident axis was estimated to be $\langle -1-16\rangle$ [Fig. 2(c)], which is 13° off from the conventional $\langle 001\rangle$ incident axis. The QDs were hardly resolved in Fig. 2(c), probably due to the greater thickness of the specimen and due to off-Bragg diffraction. However, they were observed with better

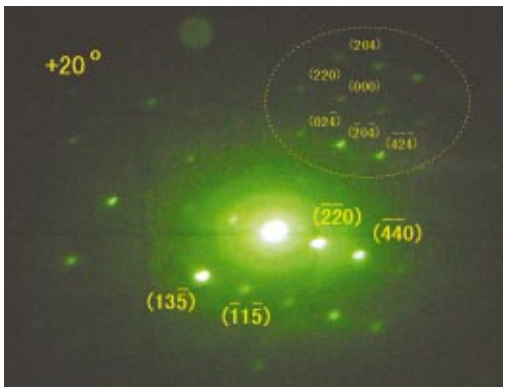

FIG. 4. (Color) Diffraction pattern for the facet-enhanced incidence. Incidence $\langle -552\rangle$ is derived from main diffraction spots, but the spots encircled suggests perturbed incidence of $\langle -221\rangle$. Indexes for encircled spots are for reference.

contrast (so-called *Z*-contrast) in the high-angle annular dark-field (HAADF) STEM image [Fig. 2(d)]. Each of the white specks in the image of Fig. 2(d) represents a single QD.

We can observe the QDs with various incident axes by $\langle 331\rangle$ axis rotation. Moreover, we can trace a specific QD with rotation; the arrows in Figs. 2(b)–2(d) point out the same single QD. It is highly potential for the investigation on the relationship among the shape of a certain nanostructure, location/surroundings, chemical composition, and lattice distortion, as described in the later section.

B. Facet-enhanced images of QDs

Among the various incident axes examined, we found particular axes with which the QDs were observed with the enhanced contrast of QD facets. With approximately 20° rotation from $\langle -110\rangle$ incidence, the QDs appeared as pyramids with one side shadowed at a high contrast against the underlying GaAs [Fig. 3(a)]. The index $\langle -552\rangle$ was assigned as the closest (within 6°) incident axis (Fig. 4), but the imperfect symmetry of the diffraction pattern suggests small off angles around $\langle -552\rangle$. The difference in electron-beam diffraction between the epitaxially grown InGaAs QDs and the underlying GaAs should be attributed to lattice distortion or strain effects,[14,27] induced by lattice mismatch between InGaAs and GaAs. We consider that the lattice distortion localizes on the QD facet surfaces, since the QDs were capped with bond-flexible *a*-Si. The diffraction around $\langle -552\rangle$ (and $\langle -332\rangle$ as described below) seems sensitive to the localized lattice distortion. It was also found that a high-contrast image of the bottom of the QDs was obtained with the incidence 40°-rotated and 56°-rotated from $\langle -110\rangle$, revealing localized lattice distortion on the (001) GaAs interface.

By taking the incident axis (observation angle) into account and fitting the facet shapes to the observed pyramid shadow, the facet structure of QDs was reconstructed, as shown in Fig. 3(b). The best fitted structure is the truncated pyramid formed by (110) and (111) facets, with a base of 28 nm and a height of 8 nm. The estimated size and shape of QDs differs from that obtained with the cross-sectional observation. The difference should be attributed to the ambiguous images of QDs in the cross-sectional observation caused by the strain effects[14,27] and overlap in depth direction. With 26° rotation from $\langle -110\rangle$ incidence (close to $\langle -332\rangle$ incidence), similar facet images of QDs were observed, where the (011) facets darkened instead of the (-101) facets [Fig. 3(c)]. The two incidences ($\langle -552\rangle$ and $\langle -332\rangle$) obtained here imply that small deviation from $\langle -221\rangle$ incidence causes such facet-enhanced images of QDs. Indeed, the perturbed diffraction pattern for $\langle -221\rangle$ incidence can be observed in Fig. 4 (encircled spots). We conclude from the diffraction pattern (Fig. 4) that the localized lattice distortion on (110) facets of QDs evokes the perturbed diffraction of $\langle -221\rangle$ incidence and results in the facet-enhanced contrast for incidences around $\langle -552\rangle$ or $\langle -332\rangle$. Additionally, we have also confirmed that very similar facet-enhanced images of the QDs were obtained with the conventional TEM observation for incidences around $\langle -552\rangle$ and $\langle -332\rangle$.

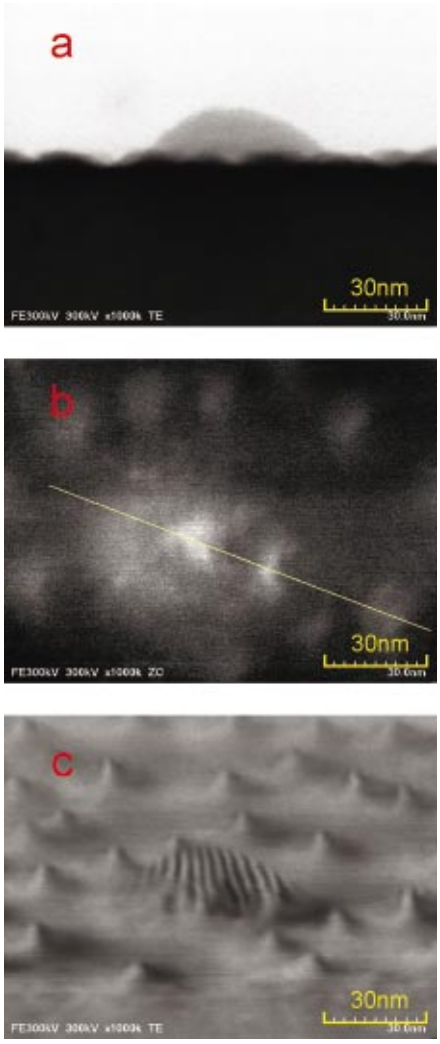

FIG. 5. (Color) Large QD observed with (a) $\langle -110 \rangle$ (bright field), (b) $\langle 0\,-13 \rangle$ (HAADF image), and (c) $\langle -552 \rangle$ (bright field) incidence. Line in (b) corresponds to the indium profile given in Fig. 7(a).

C. Indium distribution and lattice distortion

Figure 5(a) shows a bright-field STEM image of a larger QD in the same specimen, observed with $\langle -110 \rangle$ incidence. This large QD seems uniform and featureless in the cross-sectional observation. However, more detailed information on the same specific QD can be obtained in the 3D-STEM observation. In the HAADF STEM image of the QD taken with $\langle 0-13 \rangle$ incidence ($\langle 001 \rangle$-closest on-axis incidence achieved), the two bright parts were observed inside the QD as shown in Fig. 5(b). In a separate experiment with electron-energy loss spectroscopy (EELS), it was confirmed that the contrast of QDs in the HAADF-STEM images agrees very well with the indium distribution (Fig. 6). Therefore, the two bright parts in Fig. 5(b) correspond with higher-indium contents in the QD. A line profile of indium content along the line shown in Fig. 5(b) is given in Fig. 7(a). A clear indium depletion can be observed around the two indium peaks.[28]

It should be noted that the same large QD shows a featureless appearance in the cross-sectional observation [Fig. 5(a)]. This indicates that the two high-indium-content parts in Figs. 5(b) and 7(a) were buried inside the larger QD dur-

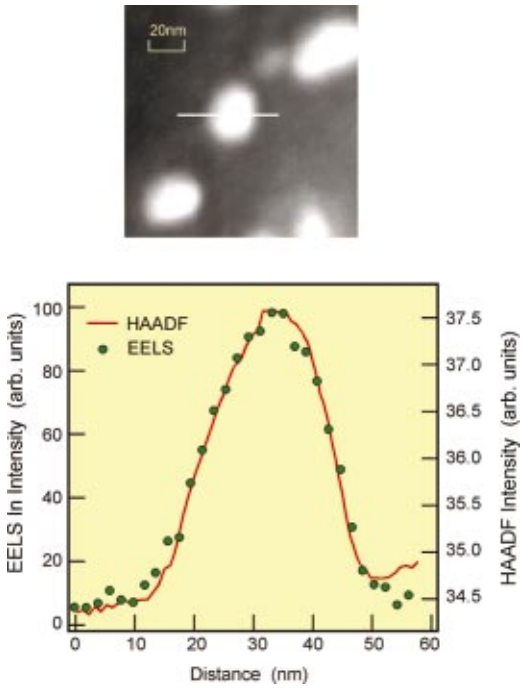

FIG. 6. (Color) Coincidence between indium signal in EELS (In *M*-edge spectrum between 460 and 520 eV, background subtracted) and intensity in HAADF-STEM image, obtained by the conventional plan-view observation of InAs/GaAs QDs. The HAADF-STEM image of QDs (top) and corresponding line-profile of HAADF-STEM intensity and EELS indium signal (bottom).

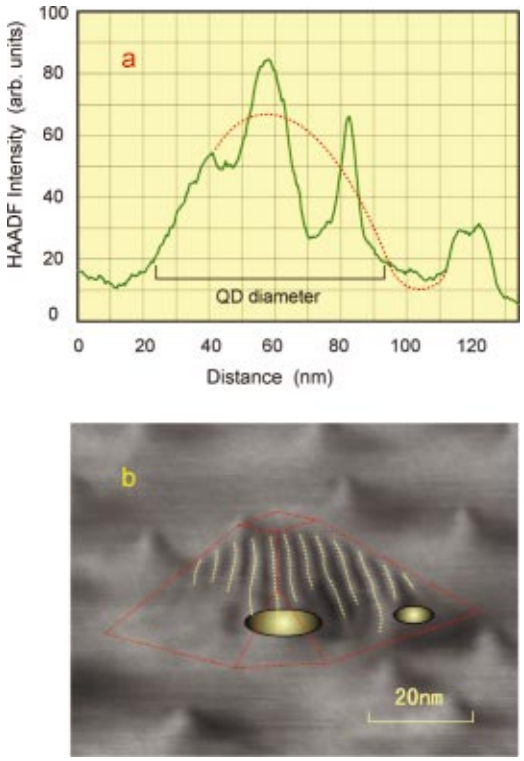

FIG. 7. (Color) (a) Line profile of indium content along the line in Fig. 5(b). Broken line gives the expectation from the uniform cross-sectional image of the QD [Fig. 5(a)]. (b) Illustration of the large QD with high-indium-content parts inside [same image of Fig. 5(c)].

ing growth. In other words, two small but high-indium-content QDs were formed at the initial stage of growth. By gathering indium atoms around themselves, they grew to coalesce into one larger QD, as is often the case in large-QD formation. The distance between the two original QDs was measured to be 25 nm from the indium peaks in Fig. 7(a), which lies within the distribution of the normal QDs in the same specimen (19–30 nm). This suggests that the higher strain around the high-indium-content QDs (but normally spaced) induces faster growth compared with the other QDs, resulting in coalescence. The height and short and long base diameters of the large QD are 18, 50, and 70 nm, respectively.

The lattice distortion due to strain relaxation with misfit dislocation is often observed as moire fringes in conventional TEM observation.[16,18] Figure 5(c) shows the bright-field STEM image of the moire fringes accompanied with the same large QD in Figs. 5(a) and 5(b), taken with incidence around $\langle -552 \rangle$. The fringe spacing is mostly uniform for the upper part of the large QD, but disarrayed for the lower right part, and disappears for the lower left part. The observation reveals the distribution of lattice relaxation inside the large QD, related to the high-indium-content parts, as illustrated in Fig. 7(b). The fringes and high-indium-content parts in Fig. 7(b) suggest that the misfit dislocation started at the edge or center of the two original QDs and propagated to the upper left side, but the strain still accumulated in the lower left side of the large QD. Since the incidence for Fig. 5(c) was $\langle -552 \rangle$, the same facet pyramid in Fig. 3(b) is applied as an eye-guide in Fig. 7(b), which seems to fit well with the upper limit of fringes. The other two large QDs we have found in the same specimen had similar lattice distortion and higher-indium contents, indicating that the large QDs were formed with the same mechanism.

It was found that the highest contrast for the moire fringes was obtained around $\langle -552 \rangle$ incidence as well as the facet-enhanced images of the QDs. The result supports our conclusion described previously that electron diffraction around $\langle -552 \rangle$ incidence (and $\langle -332 \rangle$ as well) is very sensitive to the lattice distortion of the QDs with inducing the perturbed diffraction of $\langle -221 \rangle$ incidence. It shows as well that the direct observation of indium distribution and correlated lattice relaxation inside a large QD can be performed from $\langle -552 \rangle$ or $\langle -332 \rangle$ incidences.

IV. CONCLUSIONS

We have achieved the 3D-STEM observation of InGaAs/GaAs QDs through the fabrication of a cylindrical specimen, in which both the cross-sectional and plan-view observations were performed on a single specimen. Facet-enhanced STEM images were obtained with incidences around $\langle -552 \rangle$ and $\langle -332 \rangle$, and a truncated pyramid structure with (110) and (111) facets was reconstructed. The facet-enhanced contrast is caused by the perturbed diffraction of $\langle -221 \rangle$ incidence induced by the localized lattice distortion on the (110) facets of QDs. The indium content fluctuation was directly observed inside the large QD, suggesting the coalescence of two small QDs during growth. The relaxation of lattices accompanied with the indium content fluctuation was observed as disturbed/disappeared moire fringes in the STEM images taken with the facet-enhanced incidence around $\langle -552 \rangle$.

ACKNOWLEDGMENTS

The authors would like to acknowledge Dr. M. Kouguchi, Dr. H. Kakibayashi, and Dr. H. Odagura of Hitachi Co., Ltd. for their help in performing the STEM observation and fruitful discussions. One of the authors (K.O.) thanks Ms. Mika Kurotobi very much for her continuous encouragement to complete the work. This study is supported by the Intellectual Foundation Promotion System of the Special Coordination Funds for Promoting Science and Technology of the Japanese Government for fiscal years 1997-2001.

[1] L. Roy, Appl. Phys. Lett. **79**, 3912 (2001).
[2] K. Ozasa, S. Nomura, and Y. Aoyagi, Superlattices Microstruct. **30**, 169 (2001).
[3] S. Kako, T. Sugimoto, Y. Toda, S. Ishida, A. Nishioka, and Y. Arakawa, Physica A **13**, 151 (2002).
[4] J. Urayama, TB. Norris, H. Jiang, J. Singh, and P. Bhattacharya, Appl. Phys. Lett. **80**, 2162 (2002).
[5] K. M. Kim, Y. J. Park, Y. M. Park, C. K. Hyon, E. K. Kim, and J. H. Park, J. Appl. Phys. **92**, 5453 (2002).
[6] U. Woggon, W. Langbein, J. M. Hvam, A. Rosenauer, T. Remmele, and D. Gerthsen, Appl. Phys. Lett. **71**, 377 (1997).
[7] S. Kret, T. Benabbas, C. Delamarre, Y. Androussi, A. Dubon, J. Y. Laval, and A. Lefebvre, J. Appl. Phys. **86**, 1988 (1999).
[8] N. Liu, J. Tersoff, O. Baklenov, A. L. Holmes, and C. K. Shih, Phys. Rev. Lett. **84**, 334 (2000).
[9] M. D. Giorgi, A. Passaseo, R. Rinaldi, T. Johal, R. Cingolani, A. Taurino, M. Catalano, and P. Crozier, Phys. Status Solidi B **224**, 17 (2001).
[10] D. M. Bruls, J. W. A. M. Vugs, P. M. Koenraad, H. W. M. Salemink, J. H. Wolter, M. Hopkinson, M. S. Skolnick, F. Long, and S. P. A. Gill, Appl. Phys. Lett. **81**, 1708 (2002).
[11] J. Y. Laval, S. Kret, C. Delamarre, P. Bassoul, T. Benabbas, and Y. Androussi, Microsc. Microanal. **8**, 312 (2002).
[12] M. Ishii, K. Ozasa, and Y. Aoyagi, Microelectron. Eng. (to be published).
[13] K. Georgsson, N. Carlsson, L. Samuelson, W. Seifert, and L. R. Wallenberg, Appl. Phys. Lett. **67**, 2981 (1995).
[14] S. Ruvimov and K. Scheerschmidt, Phys. Status Solidi A **150**, 471 (1995).
[15] M. Grundmann, R. Heitz, N. Ledentsov, O. Stier, D. Bimberg, VM. Ustinov, PS. Kop'ev, Zhl. Alferov, SS. Ruvimov, P. Werner, U. Gosele, and J. Heydenreich, Superlattices Microstruct. **19**, 81 (1996).
[16] F. Houzay, C. Guille, J. M. Moison, P. Henoc, and F. Barthe, J. Cryst. Growth **81**, 67 (1987).
[17] S. Guha, A. Madhukar, and K. C. Rajkumar, Appl. Phys. Lett. **57**, 2110 (1990).
[18] Y. Nabetani, A. Wakahara, and A. Sakaki, J. Appl. Phys. **78**, 6461 (1995).
[19] Y. Chen, X. W. Lin, Z. L- Weber, J. Washburn, J. F. Klem, and J. Y. Tsao, Appl. Phys. Lett. **68**, 111 (1996).
[20] K. Shiramine, Y. Horisaki, D. Suzuki, S. Itoh, Y. Ebiko, S. Muto, Y. Nakata, and N. Yokoyama, Jpn. J. Appl. Phys., Part 1 **37**, 5493 (1998).
[21] M. Koguchi, H. Kakibayashi, R. Tsuneta, M. Yamaoka, T. Niino, N. Tanaka, K. Kase, and M. Iwaki, J. Electron Microsc. **50**, 235 (2001).
[22] K. Ozasa, Y. Aoyagi, and M. Iwaki, J. Mater. Sci. Lett. (in press).
[23] K. Ozasa and Y. Aoyagi, J. Cryst. Growth **188**, 370 (1998).
[24] K. Ozasa, S. Nomura, M. Takeuchi, and Y. Aoyagi, Mater. Sci. Eng., B **86**, 34 (2001).
[25] A. J. DeMarco and J. Melngailis, J. Vac. Sci. Technol. B **19**, 2543 (2001).
[26] K. Ozasa, Y. Aoyagi, and M. Iwaki (unpublished).
[27] P. Werner, K. Scheerschmidt, N. D. Zakharov, R. Hillebrand, M. Grundmann, and R. Schneider, Cryst. Res. Technol. **35**, 759 (2000).
[28] A. Krost, F. Heinrichsdorff, D. Bimberg, J. Blasing, A. Darhuber, and G. Bauer, Cryst. Res. Technol. **34**, 89 (1999).